Landing a VTOL Unmanned Aerial Vehicle on a Moving Platform Using Optical Flow

Bruno Hérissé, Tarek Hamel, Robert Mahony, and François-Xavier Russotto

***Abstract*—This paper presents a nonlinear controller for a vertical take-off and landing (VTOL) unmanned aerial vehicle (UAV) that exploits a measurement optical flow to enable hover and landing control on a moving platform, such as, for example, the deck of a sea-going vessel. The VTOL vehicle is assumed to be equipped with a minimum sensor suite [i.e., a camera and an inertial measurement unit (IMU)], manoeuvring over a textured flat target plane. Two different tasks are considered in this paper. The first concerns the stabilization of the vehicle relative to the moving platform that maintains a constant offset from a moving reference. The second concerns regulation of automatic vertical landing onto a moving platform. Rigorous analysis of system stability is provided, and simulations are presented. Experimental results are provided for a quadrotor UAV to demonstrate the performance of the proposed control strategy.**

***Index Terms*—Automatic landing, nonlinear control, optical flow, unmanned aerial vehicle (UAV).**

I. Introduction

RECENT advances in technology and a long list of potential applications have led to a growing interest in aerial robotic vehicles [1]. Unmanned aerial vehicles (UAVs) are an ideal solution for many indoor and outdoor applications that presently jeopardize human or material safety, such as, for example, monitoring traffic congestion, regular inspection of infrastructure such as bridges, dam walls, and power cables, investigation of hazardous environments, etc. An important capability for a subset of potential applications, particularly those associated with maritime scenarios, is the ability to autonomously land the vehicle on a moving platform such as the deck of a sea-going vessel, or, indeed, any landing pad that is attached to a moving vehicle. The associated capability of stabilizing the motion of the UAV with respect to a dynamic moving environment is itself of significance in a wide range of more general applications. Autonomous landing of UAV on moving platforms has been investigated using a model of the vertical motion of landing platform [2], [3], a tether guide [4], or known target motion [5], [6]. The main idea of prior work is based on obtaining a prediction of the motion of the moving landing pad to provide a feed-forward compensation during the landing manoeuvre. This approach has the advantage that, should a reliable predictive model of the motion of the landing pad be determined, the resulting performance of the landing manoeuvre is of high quality. The approach suffers from the disadvantage that in many applications of interest, it is difficult to determine a reliable predictive model of the motion of the landing pad either because the motion of the landing pad is primarily stochastic, and no predictive model is valid, or because of the limited amount of data available to the UAV during the landing manoeuvre. In such situations, the vehicle control algorithm must fall back on feedback-control strategies. An approach that stems from the insight into the behavior of flying insects and animals uses visual flow [7] as feedback for aerial vehicles in the control of motion in dynamic environments. Since optical flow provides relative velocity and proximity information with respect to the local environment [8], it is an ideal cue that can be used to perform landing-control strategies [7], [9], as well as obstacle avoidance [10]–[12], terrain following [13]–[15], visual servo control [16], or even in both localization and control [17]. It is rare that moving obstacles are considered in prior literature using optical flow; however, it is well known that insects show great capabilities in achieving landing tasks on moving objects such as, for example, a bee landing on a flower. Moreover, the full vehicle dynamics analysis is rarely discussed in the majority of work on the analysis of insect flight behavior, since the flight regime of insects is highly damped due to their high drag-to-mass ratios. The control strategies that have been observed in the various biological studies do not necessarily generalize to high-inertia, low-drag aerial vehicles.

In this paper, an optical-flow-based control law for hovering flight and landing manoeuvre on a moving platform is proposed using only on inertial measurement unit (IMU) and optical-flow measurements. The image information that is considered is the average optical flow that is obtained from a textured target plane, using additional information provided by an embedded IMU for *derotation* of the flow. A nonlinear proportional-integral (PI)-type controller is designed for hovering flight, while another nonlinear controller, exploiting the vertical optical flow (similar to the inverse of the well-known time-to-contact), is proposed for vertical landing. It is necessary to assume bounded dynamics of the moving platform; however, no predictive model of the platform is required to obtain the desired closed-loop performance.

Manuscript received July 6, 2010; revised March 30, 2011; accepted July 27, 2011. Date of publication September 12, 2011; date of current version February 9, 2012. This paper was recommended for publication by Associate Editor M. Sitti and Editor G. Oriolo upon evaluation of the reviewers' comments. This work was supported in part by Naviflow grant, by Agence Nationale de la Recherche project SCUAV (ANR-06-ROBO-0007), and by the Australian Research Council through the ARC Discovery Project DP0880509 entitled "Image-based teleoperation of semi-autonomous robotic vehicles."

B. Hérissé is with the ONERA—The French Aerospace Lab, Palaiseau Cedex F-91123, France (e-mail: bruno.herisse@onera.fr).

T. Hamel is with the I3S UNSA-CNRS Laboratory, University of Nice Sophia Antipolis, Sophia Antipolis Cedex 06903, France (e-mail: thamel@i3s.unice.fr).

R. Mahony is with the Research School of Engineering, Australian National University, Canberra, A.C.T 0200, Australia (e-mail: Robert.Mahony@anu.edu.au).

F.-X. Russotto is with the CEA List, Interactive Robotics Laboratory Fontenay-aux-Roses 92265, France (e-mail: francois-xavier.russotto@cea.fr).

This paper has supplementary downloadable material available at http://ieeexplore.ieee.org.

Color versions of one or more of the figures in this paper are available online at http://ieeexplore.ieee.org.

Digital Object Identifier 10.1109/TRO.2011.2163435

To prove global stability and convergence of the closed-loop system, Lyapunov analysis is used both for the stabilization of the hovering flight relative to a static plane and for the vertical landing relative to a horizontal plane moving with unknown (bounded) dynamics in the vertical direction. In practice, the stabilization and vertical landing also work with lateral motion. Experimental results are obtained on a quad-rotor UAV capable of quasi-stationary flight that is developed at French Atomic Energy Commission (CEA). A "high-gain" controller is used to stabilize the orientation dynamics of the vehicle, an approach classically known in aeronautics as guidance and control (or hierarchical control) [18], and the stabilization and landing control are developed for the resulting reduced translational dynamics of the vehicle. The proposed closed-loop control schemes demonstrate efficiency and performance for the hovering flight and vertical landing manoeuvre.

The material presented in this paper is an extension of the prior work [19]. It incorporates the ground effect, considers the situation of target is moving, contains detailed proof of the system stability, and incorporates additional simulations and experiments.

This paper consists of six sections followed by a conclusion. Section II presents the fundamental equations of motion for an X4-flyer UAV. In Section III, fundamental equations of optical flow are presented. Sections IV and V present the proposed control strategies for hovering and vertical landing manoeuvre, respectively. Section VI describes simulations results, and Section VII describes the experimental results that are obtained on the quad-rotor vehicle.

II. Unmanned Aerial Vehicle Dynamic Model and Time-Scale Separation

The vertical take-off and landing (VTOL) UAV is represented by a rigid body of mass m and of tensor of inertia $\mathbf{I}$ along with external forces due to gravity and forces and torques provided by rotors. To describe the motion of the UAV, two reference frames are introduced: an inertial reference frame $\mathcal{I}$ associated with the vector basis $[e_1, e_2, e_3]$ and a body-fixed frame $\mathcal{B}$ attached to the UAV at the center of mass and associated with the vector basis $[e_1^b, e_2^b, e_3^b]$. The position and the linear velocity of the UAV in $\mathcal{I}$ are, respectively, denoted $\xi = (x, y, z)^T$ and $v = (\dot{x}, \dot{y}, \dot{z})^T$. The orientation of the UAV is given by the orientation matrix $R \in SO(3)$ from $\mathcal{B}$ to $\mathcal{I}$. Finally, let $\Omega = (\Omega_1, \Omega_2, \Omega_3)^T$ be the angular velocity of the UAV that is defined in $\mathcal{B}$.

A translational force F and a control torque Γ are applied to the UAV. The translational force F combines thrust, lift, drag, and gravity components. For a miniature VTOL UAV in quasi-stationary flight, one can reasonably assume that the aerodynamic forces are always in direction e_3^b, since the thrust force predominates over other components [20]. The gravitational force can be separated from other forces, and the dynamics of the VTOL UAV can be written as

$$\dot{\xi} = v \tag{1}$$

$$m\dot{v} = -TRe_3 + mge_3 + \Delta \tag{2}$$

$$\epsilon\dot{R} = R\bar{\Omega}_\times, \quad \bar{\Omega} = \epsilon\Omega \tag{3}$$

$$\epsilon\mathbf{I}\dot{\bar{\Omega}} = -\bar{\Omega} \times \mathbf{I}\bar{\Omega} + \bar{\Gamma}, \quad \bar{\Gamma} = \epsilon^2\Gamma. \tag{4}$$

In the aforementioned notation, g is the acceleration due to gravity, and T is a scalar input that is termed the thrust or heave, which is applied in direction $e_3^b = Re_3$, i.e., the third-axis unit vector. The term Δ represents constant (or slowly time-varying unmodeled) forces. The matrix $\Omega_\times$ denotes the skew-symmetric matrix associated with the vector product $\Omega_\times x := \Omega \times x$ for any x.

The positive parameter $0 < \epsilon < 1$ is introduced for time-scale separation between the translation and orientation dynamics. It means that the orientation dynamics of the VTOL UAV are compensated with separate high-gain control loop ($\Gamma = \bar{\Gamma}/\epsilon^2$). For this hierarchical control, the time-scale separation between the translational dynamics (slow time scale) and the orientation dynamics (fast time scale) can be used to design position and orientation controllers under simplifying assumptions. Although reduced-order subsystems can, hence, be considered for control design, the stability must be analyzed by considering the complete closed-loop system [18]. In this paper, however, we will focus on the control design for the translational dynamics.

Thus, the full vectorial term TRe_3 will be considered as control input for these dynamics. We will assign its desired value $u \equiv (TRe_3)^d = T^dR^de_3$. Assuming that actuator dynamics can be neglected, the value T^d is considered to be instantaneously reached by T. For the orientation dynamics of (3) and (4), a high-gain controller is used to ensure that the orientation R of the UAV converges to the desired orientation R^d. The resulting control problem is simplified to

$$\dot{\xi} = v, \; m\dot{v} = -u + mge_3 + \Delta. \tag{5}$$

Thus, we consider only control of the translational dynamics (5) with a direct control input u. This common approach is used in practice and may be justified theoretically using singular perturbation theory [21].

III. Optical-Flow Equations

In this section, image plane kinematics and spherical optical flow are derived. The camera is assumed to be attached to the center of mass of the vehicle so that the camera frame coincides with the body-fixed frame.

A. Kinematics of an Image Point Under Spherical Projection

We compute optical flow in spherical coordinates in order to exploit the passivity-like property that is discussed in [22]. The main advantage is that, in spherical coordinates, the optical flow is expressed in a simple form. Moreover, it is shown in [23] that optical-flow equations can be numerically computed from an image plane to a spherical retina. A Jacobian matrix relates temporal derivatives (velocities) in the spherical coordinate system to those in the image frame. Motivated by this discussion, we make the assumption that the image surface of the camera is spherical with unit image radius.

Define $P = (X, Y, Z) \in \mathbb{R}^3$ as a visible target point, possibly moving, expressed in the camera frame. The image point that is observed by the spherical camera is denoted p and is the

Fig. 1. Quadrotor UAV developed in Centre d'Energie Atomique and used for the experimental results in this paper.

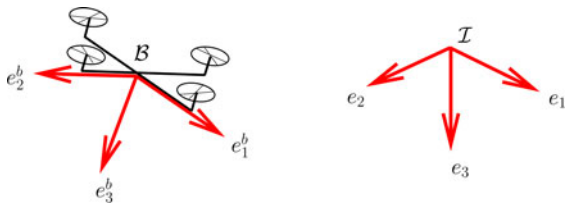

Fig. 2. Definition of the body-fixed frame $\mathcal{B}$ and the inertial frame $\mathcal{I}$.

projection of P onto the image surface $\mathcal{S}^2$ of the camera. Thus

$$p = \frac{P}{\|P\|}. \tag{6}$$

The time derivative $\dot{p}$ is the kinematics of the image point, which is also called optical-flow equations, on the spherical surface. The kinematics of an image point for a spherical camera of image surface radius unity are [8], [22]

$$\dot{p} = -\Omega \times p - \frac{\pi_p}{\|P\|}(V - V_P) \tag{7}$$

where $\pi_p = (I_3 - pp^\top)$ is the projection $\pi_p : \mathbb{R}^3 \to T_p\mathcal{S}^2$, i.e., the tangent space of the sphere $\mathcal{S}^2$ at the point $p \in \mathcal{S}^2$. The vectors $V = R^\top v$ and V_P are expressed in the body-fixed frame and represent, respectively, the translational velocity of the center of mass of the vehicle and the translational velocity of the target point P.

Let $\eta \in \mathcal{I}$ denote the unit normal of a target plane [16] (see Fig. 3). Define $d := d(t)$ to be the orthogonal distance from the target surface to the origin of frame $\mathcal{B}$ that is measured as a positive scalar. Thus, for any point P on the target surface

$$d(t) = \langle P, R^\top \eta \rangle$$

where P is expressed in the body-fixed frame, and η is expressed in the inertial frame. For a target point, one has

$$\|P\| = \frac{d(t)}{\langle p, R^\top \eta \rangle} = \frac{d(t)}{\cos(\theta)}$$

where θ is the angle between the inertial direction η and the observed target point p. Substitution of this relationship into (7)

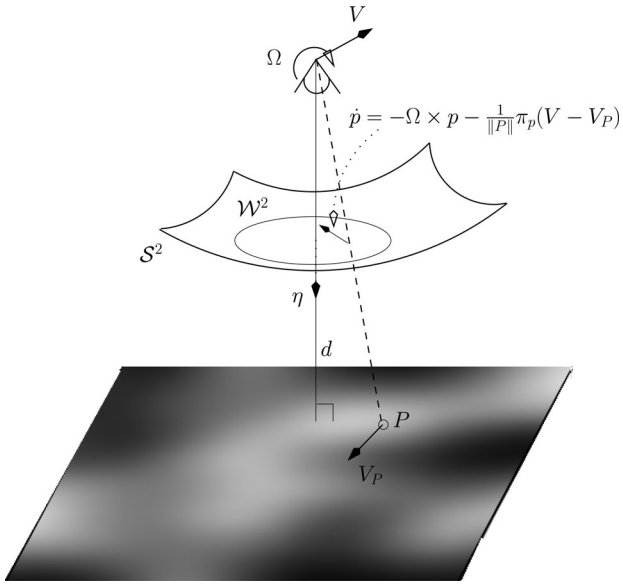

Fig. 3. Image kinematics for spherical camera image geometry.

yields

$$\dot{p} = -\Omega_\times p - \frac{\cos(\theta)}{d(t)}\pi_p(V - V_P). \tag{8}$$

B. Average Optical Flow

Measuring the optical flow is a key aspect of the practical implementation of the control algorithms that are proposed in the sequel. The optical flow $\dot{p}$ can be computed using a range of algorithms (such as correlation-based techniques, features-based approaches, differential techniques, etc.) [24]. Note that because of the rotational ego-motion of the camera, (8) involves the angular velocity as well as the linear velocity [8]. For the control problem, we define an inertial average optical flow from the integral of all observed optical flow that is corrected for rotational angular velocity. By integrating optical flow over an aperture, which in this case is a solid angle on the sphere, we obtain information on the scaled velocity of the vehicle.

We assume that the target is a textured plane moving with a pure translational velocity $V_t \in \mathcal{B}$ (no rotational velocity). Thus, for any target points P on the plane, $V_P = V_t$. We also assume that the normal direction η is known and the available data are $\dot{p}$, R, and Ω, where R and Ω are estimated from the IMU data [25]. The average optical flow is obtained by integrating the observed optical flow over a solid angle $\mathcal{W}^2$ of the sphere around the pole normal to the target plane (see Fig. 3). The average of the optical flow on the solid angle $\mathcal{W}^2$ is given by (see the Appendix for more details)

$$\phi = \iint_{\mathcal{W}^2} \dot{p}\, dp = -\pi (\sin\theta_0)^2\, \Omega \times R^\top \eta - \frac{Q(V - V_t)}{d} \tag{9}$$

where the parameter θ_0 and the matrix Q depend on the size of the solid angle $\mathcal{W}^2$. It can be verified that $Q = R^\top(R_t \Lambda R_t^\top)R$ is a symmetric positive-definite matrix. The matrix Λ is a constant diagonal matrix that depends on parameters of the solid angle $\mathcal{W}^2$, and R_t represents the orientation matrix of the target plane

with respect to the inertial frame. For instance, if $\mathcal{W}^2$ is the hemisphere centered at η, corresponding to the visual image of the infinite target plane, it can be shown that [16]

$$\Lambda = \frac{\pi}{4}\begin{pmatrix} 3 & 0 & 0 \\ 0 & 3 & 0 \\ 0 & 0 & 2 \end{pmatrix}. \tag{10}$$

From (9), it is straightforward to obtain a measurement of the inertial average optical flow corrected for rotational angular velocity

$$w = -(R_t \Lambda^{-1} R_t^\top) R(\phi + \pi (\sin\theta_0)^2\, \Omega \times R^\top \eta). \tag{11}$$

By expressing with respect to the rigid-body motion, it yields

$$w = \frac{v - v_t}{d} + \text{noise} \tag{12}$$

where $v_t = RV_t$ is the translational velocity of the target plane that is expressed in the inertial frame. Note that for theoretical analysis that is provided in Sections IV and V, the noise of (12) is ignored. Its effects on the convergence is considered in Section VI.

Remark 3.1: In the particular situation where the target plane is stationary ($v_t = 0$), (12) becomes

$$w = \frac{v}{d} + \text{noise}. \tag{13}$$

IV. Stabilization of the Hovering Flight Over a Textured Target

In this section, a control design that ensures hovering flight over a textured flat plane is proposed. The control problem that is considered is the stabilization of the linear velocity about zero despite unmodeled constant (or slowly time-varying) dynamics. In particular, the velocity of the target will be assumed to be constant ($\dot{v}_t \equiv 0$). A PI-type nonlinear controller that depends only on the measurable variable $w = (v - v_t)/d = \tilde{v}/d$ (12) is proposed for the translational dynamics (5). The result is stated in the following theorem.

Theorem 4.1: Assume that η is known and invariant, and Δ is a constant. Consider the dynamics (5), and assume that the control input u is chosen as

$$u = k_P w + k_I \int_0^t w d\tau + mge_3, \quad k_P, k_I > 0. \tag{14}$$

Then, for any initial conditions $d_0 = d(0) > 0$, the linear velocity error $\tilde{v}$ converges asymptotically to zero. More precisely, we have the following

1) $\dot{d} = -\langle \tilde{v}, \eta \rangle$ converges to 0 and $d(t) > 0,\ \forall t \geq 0$.
2) The horizontal velocity $\tilde{v}^\parallel = \pi_\eta \tilde{v}$ converges to zero.

Proof:

Proof of item 1: Recall the dynamics of the vehicle (5) and consider the component $\tilde{v}^\perp = \langle \tilde{v}, \eta \rangle$ in direction η. One obtains

$$m\dot{\tilde{v}}^\perp = -k_P \frac{\tilde{v}^\perp}{d} - k_I \int_0^t \frac{\tilde{v}^\perp}{d} d\tau + \langle \Delta, \eta \rangle. \tag{15}$$

Note that $\tilde{v}^\perp = -\dot{d}$. Equation (15) can also be written as follows:

$$m\ddot{d} = -k_P \frac{\dot{d}}{d} - k_I \int_0^t \frac{\dot{d}}{d} d\tau - \langle \Delta, \eta \rangle \tag{16}$$

$$= -k_P \frac{\dot{d}}{d} - k_I \ln\left(\frac{d}{d_\infty}\right) \tag{17}$$

where $d_\infty = d_0 e^{-\langle \Delta, \eta \rangle / k_I}$. Note that the control law is well defined and smooth for $d > 0$. For any initial conditions, such that $d_0 = d(0) > 0$, define the Lyapunov function candidate $\mathcal{L}_\eta$ by

$$\mathcal{L}_\eta = \frac{m}{2d_\infty}\dot{d}^2 + k_I \left[\frac{d}{d_\infty}\left(\ln\left(\frac{d}{d_\infty}\right) - 1\right) + 1\right] \geq 0. \tag{18}$$

Since function $u \mapsto (u(\ln u - 1) + 1) \geq 0\ \forall u > 0$, it is straightforward to verify that $\mathcal{L}_\eta \geq 0$. Differentiating $\mathcal{L}_\eta$ and recalling (17), one obtains

$$\dot{\mathcal{L}}_\eta = -k_P \frac{\dot{d}^2}{d d_\infty}. \tag{19}$$

This implies that $\mathcal{L}_\eta < \mathcal{L}_\eta(0)$, as long as $d(t) > 0$. Two different cases may occur depending on the initial value of $\mathcal{L}_\eta$: $\mathcal{L}_\eta(0) < k_I$ and $\mathcal{L}_\eta(0) \geq k_I$. From the expression of the Lyapunov function (18), the first case ($\mathcal{L}_\eta(0) < k_I$) implies that there exists $\varepsilon > 0$ such that $d(t) > \varepsilon > 0\ \forall t$. Consequently, d remains strictly positive, and (17) is well defined for all time. Application of LaSalle's principle shows that the invariant set is contained in the set that is defined by $\dot{\mathcal{L}}_\eta = 0$. This implies that $\dot{d} \equiv 0$ in the invariant set. Recalling (17), it is straightforward to show that d converges asymptotically to d_∞.

For the second situation ($\mathcal{L}_\eta(0) \geq k_I$), we have to show that $d \neq 0$ for all time. Assume that there exists a first time t_1 such that $\dot{d}(t_1) < 0$ and $0 < d(t_1) < d_\infty$. If we show that there exists a second time $t_2 > t_1$ such that $\dot{d}(t_2) = 0$ and $d(t_2) > 0$, then $\mathcal{L}_\eta(t_2) < k_I$ and conditions of the first case are verified, and the result follows. We proceed using a proof by contradiction. Assume that for all time $t > t_1$, $\dot{d}(t) < 0$. This implies $d(t) < d(t_1) < d_\infty\ \forall t > t_1$. Thus, recalling (17), it follows that there exists $\varepsilon > 0$ such that $\ddot{d}(t) > \varepsilon > 0\ \forall t > t_1$. As a consequence, there exists a time $T > t_1$ such that d converges to 0 ($d \geq 0$) when t tends to T. Recalling (17), it yields

$$\ddot{d} > -\frac{k_P}{m}\frac{\dot{d}}{d} > 0 \quad \forall t > t_1. \tag{20}$$

Integrating this equation, it follows that

$$\dot{d} - \dot{d}(t_1) > -\frac{k_P}{m} \ln\left(\frac{d}{d(t_1)}\right) \forall t > t_1. \tag{21}$$

Since d converges to 0, $\dot{d}$ converges to $+\infty$. This contradicts the fact that $\dot{d} < 0\ \forall t > t_1$. It follows that $d(t) > 0\ \forall t \geq 0$, and consequently, $d(t)$ converges to d_∞.

Proof of item 2: Let $\tilde{v}^\parallel$ be the planar velocity $\pi_\eta \tilde{v} \in \mathcal{I}$. Consider the component perpendicular to η of the control law (14)

$$u^\parallel = \pi_\eta u = k_P \frac{\tilde{v}^\parallel}{d} + k_I \int_0^t \frac{\tilde{v}^\parallel}{d} d\tau + mg\pi_\eta e_3. \tag{22}$$

Recall the dynamics of the vehicle (5) and consider the component perpendicular to η. Substituting the control law (22) into (5), one obtains

$$m\dot{\tilde{v}}^{\parallel} = -k_P \frac{\tilde{v}^{\parallel}}{d} - k_I \int_0^t \frac{\tilde{v}^{\parallel}}{d}\, d\tau + \Delta^{\parallel} \tag{23}$$

where $\Delta^{\parallel} = \pi_\eta \Delta$. Let δ_1 be the following variable:

$$\delta_1 = \int_0^t \frac{\tilde{v}^{\parallel}}{d}\, d\tau - \frac{\Delta^{\parallel}}{k_I}. \tag{24}$$

Differentiating δ_1, it yields

$$\dot{\delta}_1 = \frac{\tilde{v}^{\parallel}}{d}. \tag{25}$$

Consider the following Lyapunov function candidate:

$$\mathcal{L}_{\pi_\eta} = k_I \frac{\|\delta_1\|^2}{2} + m\frac{\|\delta_2\|^2}{2} \tag{26}$$

where $\delta_2 = \tilde{v}^{\parallel}/\sqrt{d}$. Differentiating $\mathcal{L}_{\pi_\eta}$ and recalling (23), one obtains

$$\dot{\mathcal{L}}_{\pi_\eta} = -\|\delta_2\|^2 \frac{\left(k_P + m\dot{d}/2\right)}{d} \tag{27}$$

Using the fact that $(d, \dot{d})$ converges to $(d_\infty, 0)$, one can ensure that there exists a time T and $\varepsilon > 0$ such that

$$\frac{(k_P + m\dot{d}/2)}{d} > \varepsilon > 0 \quad \forall t > T.$$

Therefore, $\dot{\mathcal{L}}_{\pi_\eta} < -\varepsilon \|\delta_2\|^2,\ \forall t > T$. Moreover, it is straightforward to verify that $\mathcal{L}_{\pi_\eta}$ remains bounded in $[0, T]$ by noticing that

$$\dot{\mathcal{L}}_{\pi_\eta} < \frac{|\dot{d}|_{\max}}{d_{\min}} \mathcal{L}_{\pi_\eta} \quad \forall t \in [0, T].$$

This implies that $\mathcal{L}_{\pi_\eta}(t) < \mathcal{L}_{\pi_\eta}(T),\ \forall t > T$. To show that δ_2 converges to 0, we need to show that $\dot{\mathcal{L}}_{\pi_\eta}$ is uniformly continuous. Then, application of Barbalat's Lemma (see [21]) will conclude the proof. To this purpose, it is sufficient to show that $\ddot{\mathcal{L}}_{\pi_\eta}$ is bounded. Since $\dot{d}$ and $\ddot{d}$ are bounded, it remains to show that δ_2 and $\dot{\delta}_2$ are bounded to satisfy the condition. δ_1 and δ_2 are bounded since $\mathcal{L}_{\pi_\eta}$ is bounded. Moreover, it is straightforward to show that $\dot{\delta}_2$ is bounded using its expression:

$$\dot{\delta}_2 = -\frac{k_P}{md}\delta_2 - \frac{k_I}{m\sqrt{d}}\delta_1 - \frac{1}{2}\frac{\dot{d}}{d}\delta_2.$$

Thus, $\dot{\mathcal{L}}_{\pi_\eta}$ is uniformly continuous; hence, δ_2 converges to 0.

Finally, using the fact that $\tilde{v} = \tilde{v}^{\perp}\eta + \tilde{v}^{\parallel}$, it follows that $\tilde{v}$ converges to zero. ∎

V. Landing Control on a Moving Textured Target

In this section, we consider the landing manoeuvre of the aerial robot on a horizontal plane that moves vertically. The primary goal is to address the question of the vertical landing on a moving platform (target) with unknown dynamics. The most important application concerns landing on a deck of a ship in high seas and tough weather [2], [4]–[6]. A common model of the vertical motion z_G of the platform as the motion of the ship involved by the sea waves is [2]

$$z_G = \sum_{i=1}^{n} a_i \cos(\omega_i t + \phi_i) \tag{28}$$

where $a_i,\ \omega_i,$ and ϕ_i are unknown constants. The classical approach estimates the parameters of motion and uses these to add a feed-forward compensation term in the control input. In this paper, we consider a more general vertical motion z_G of the platform with respect to the inertial frame $\mathcal{I}$. We assume that z_G is a smooth function of class $\mathcal{C}^2$ (z_G and $\dot{z}_G$ are continuous functions of time t) such that $\ddot{z}_G$ is bounded by a known value.

We assume that the target plane belongs to the plane x–y of the inertial frame so that $d \equiv h$ is the height of the vehicle with respect to the moving platform. The vertical velocity of the target plane is $\dot{z}_G e_3$. Consequently, from (12) with $v_t^{\perp} = \dot{z}_G e_3$, it is straightforward to verify that

$$w^{\perp} = \langle w, e_3 \rangle = \frac{v^{\perp} - \dot{z}_G e_3}{h}.$$

Hence

$$w_z = w^{\perp} = -\frac{\dot{h}}{h}. \tag{29}$$

Define

$$w^d = (0, 0, \omega^*)^T,\ \ \omega^* > 0$$

as the desired average optical flow. Note that the vertical component of the inertial average optical flow acts analogously to optical-flow divergence. It is straightforward to show that if $w \equiv w^d$, one has $(v_x, v_y) = (0, 0)$ and $v_z = h_0\omega^* \exp(-\omega^* t)$. Consequently, $h(t) = h_0 \exp(-\omega^* t)$ that ensures a smooth vertical landing. In practice, it is impossible to exactly track ω^*, and it is necessary to implement a feedback system.

We propose to use the previous control law (14) for the x–y dynamics to stabilize the vehicle over the landing pad. We still need to provide a control scheme for the remaining degree of freedom ($h \equiv |z - z_G|$). In particular, we fix a desired set point ω^* for the flow divergence (i.e., the flow in the normal direction to the target plane, which is equal to the inverse of the time-to-contact) and design a control law that regulates $(\dot{h}/h + \omega^*)$ around 0. The controller is a direct application of the controller that is proposed in [26], along with a complete and more rigorous proof of the exponential convergence and stability of $(h, \dot{h})$ to $(0, 0)$ despite unknown dynamics and unknown terms. Consider the dynamics

$$m\dot{v} = -b(t)u + mge_3 + \Delta(t) \tag{30}$$

where $b(t)$ is a slowly time-varying parameter that models the ground effect ($b \geq 1$). An approximate model for $b(t)$ can be found in [20], [27]

$$\frac{1}{b(t)} = 1 - \left(\frac{D_0}{h(t) + l_0}\right)^2 \tag{31}$$

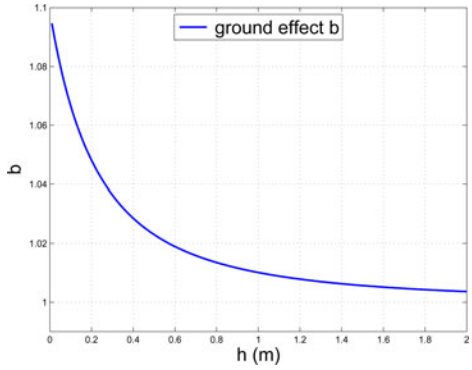

Fig. 4. Ground effect b with $l_0 = 0.5$ m and $D_0 = 0.15$ m.

where l_0 and D_0 can be identified on a physical system. Note that $l_0 > D_0$ so that $b > 1$ when $h = 0$ (see Fig. 4). Note also that $\max(b(t)) = b_{\max}$ is obtained when $h = 0$.

Theorem 5.1: Consider the dynamics of the vertical component of (30), and assume that the vertical component u_z of the thrust vector u is the control input. Choose u_z as

$$u_z = mk(w_z - \omega^*) + mg. \tag{32}$$

Assume that z_G is at least $\mathcal{C}^2$, assume that $\ddot{z}_G, \Delta(t)$ are bounded and uniformly continuous, and assume that $b(t) \geq 1$. Choose the control gain k such that

$$k > \frac{|\Delta_z|_{\max} + m|\ddot{z}_G|_{\max} + mg\,|b_{\max} - 1|}{m\omega^*}. \tag{33}$$

Then, for all initial conditions, such that $h_0 > 0$ ($h_0 \equiv |z(0) - z_G(0)|$), we have the following.

1) The third component of the differential equation (30) along with (32) is smooth and nonsingular. This implies that the solution $(h(t), \dot{h}(t))$ is well defined for all time $t \geq 0$.
2) $h(t) > 0$ remains positive, and $(h, \dot{h})$ converge exponentially to zero.
3) The control law (32) is bounded for all time and $\ddot{h} \to 0$.

Proof: In the first step, we prove that the third component of the differential equation (30) along with (32) is smooth and nonsingular while $h(t) > 0$. This implies that there exists a time $T_{\max} > 0$ such that the solution $(h(t), \dot{h}(t))$ exists and is well defined on $t \in [0, T_{\max})$. In a second step, we prove item 2 while showing that $T_{\max} = \infty$, and finally, we will prove item 3.

Proof of item 1 for $t \in [0, T_{\max})$:

First, recall that the dynamics of the considered system are decoupled, and recall the dynamics of the third component of (30)

$$m\dot{v}_z = -b(t)u_z + mg + \Delta_z(t). \tag{34}$$

It follows that the height dynamics can be written as follows:

$$m\ddot{h} = mkb(t)(w_z - \omega^*) - \Delta_z + (b(t) - 1)mg + m\ddot{z}_G \tag{35}$$

$$= -mkb(t)\left(\frac{\dot{h}}{h} + \alpha(t)\right) \tag{36}$$

where

$$\alpha(t) = \left(\omega^* + \frac{\Delta_z}{mkb(t)} - (b(t) - 1)\frac{g}{kb(t)} - \frac{\ddot{z}_G}{kb(t)}\right). \tag{37}$$

Recalling condition (33), it is straightforward to show that $\alpha(t)$ is a positive and bounded function ($\alpha(t) > 0,\ \forall t \geq 0$).

The dynamics (36) are well defined as long as $h(t) > 0$; hence, there exists a first time $T_{\max}$, possibly infinite, such that $(h, \dot{h})$ is well defined on $[0, T_{\max})$.

Proof of item 2 for $t \in [0, T_{\max})$:

Define the following virtual state on $[0, T_{\max})$

$$\zeta(t) = h(t)\exp\left(\int_0^t \frac{\ddot{h}(\tau)}{kb(\tau)}\,d\tau\right). \tag{38}$$

Differentiating ζ and recalling (36) yields

$$\dot{\zeta} = -\alpha\zeta. \tag{39}$$

Since $\zeta_0 = h_0$, it follows that on $[0, T_{\max})$

$$h_0 \exp(-\alpha_{\max} t) < \zeta(t) < h_0 \exp(-\alpha_{\min} t).$$

It remains to show that $\left|\int_0^t \frac{\ddot{h}(\tau)}{kb(\tau)}\,d\tau\right|$ is bounded on $[0, T_{\max})$ to ensure, using (38), that there exist $\epsilon_1, \epsilon_2 > 0$ such that

$$\epsilon_1 h_0 \exp(-\alpha_{\max} t) < h(t) < \epsilon_2 h_0 \exp(-\alpha_{\min} t)$$

for all time $t \in [0, T_{\max})$. We will show that $T_{\max} = \infty$ using continuity. This will ensure that $(h, \dot{h})$ is well defined on $[0, \infty)$ and that $h(t)$ converges exponentially to 0.

To do this, we must prove that $\left|\int_0^t \frac{\ddot{h}(\tau)}{kb(\tau)}\,d\tau\right|$ is bounded by studying the evolution of $(\dot{h}, \ddot{h})$.

Proof that the sign of $\dot{h}(t)$ does not change more than once and $|\dot{h}(t)|$ is bounded. Two situations may occur.

1) $\dot{h}(0) \geq 0$: To show that there exists a time T on $[0, T_{\max})$ such that $\dot{h}(T) < 0$, assume the converse, that is, $\dot{h} \geq 0$ for all time t. Thus, from (36) where $\alpha(t) > 0$, $\ddot{h} < 0$ and, by exploiting (38) where $b \geq 1$

$$\zeta(t) \geq h\exp\left(\frac{\dot{h}(t) - \dot{h}_0}{k}\right) \geq h_0 \exp\left(-\frac{\dot{h}_0}{k}\right).$$

Since $\dot{\zeta} < -\alpha_{\min}\zeta$, it follows that ζ is exponentially decreasing. Therefore, there exists a time T such that $\zeta(T) < h_0 \exp(-\dot{h}_0/k)$. This contradicts the assumption.

2) $\dot{h}(0) < 0$: to show that $\dot{h} < 0,\ \forall t \in [0, T_{\max})$, assume the converse; that is, there exists T such that $\dot{h}(T) = 0$ and $\dot{h}(t) < 0,\ \forall t < T$. Since $\dot{h}$ is continuous and recalling (36), it follows that there exists $\delta > 0$ and $\epsilon > 0$ such that $\ddot{h}(t) < -\epsilon,\ \forall t \in [T - \delta, T]$. Recalling (38), one has that

$$\zeta(t) = h(t)\exp\left(\int_0^{T-\delta} \frac{\ddot{h}(\tau)}{kb(\tau)}\,d\tau + \int_{T-\delta}^t \frac{\ddot{h}(\tau)}{kb(\tau)}\,d\tau\right).$$

Using the fact that $\ddot{h}(t) < -\epsilon\ \forall t \in [T - \delta, T]$, it follows that

$$\zeta(t) < h(t)\exp\left(\int_0^{T-\delta} \frac{\ddot{h}(\tau)}{kb(\tau)}\,d\tau\right)\ \forall t \in [T - \delta, T].$$

Moreover, since $b(t) \geq 1\ \forall t \in [0, T_{\max})$

$$\zeta(t) \geq h(t) \exp\left(\int_0^{T-\delta} \frac{\ddot{h}(\tau)}{kb(\tau)}\, d\tau + \int_{T-\delta}^{t} \frac{\ddot{h}(\tau)}{k}\, d\tau\right)$$

$$\geq h(t) \exp\left(\int_0^{T-\delta} \frac{\ddot{h}(\tau)}{kb(\tau)}\, d\tau\right) \exp\left(\frac{\dot{h}(t)}{k}\right).$$

Using the fact that $\dot{h}(T) = 0$, one obtains

$$\zeta(T) \geq h(T) \exp\left(\int_0^{T-\delta} \frac{\ddot{h}(\tau)}{kb(\tau)}\, d\tau\right).$$

This proves the contradiction.

To show that $\dot{h}$ is lower bounded, let $\mathcal{J}$ be the following storage function:

$$\mathcal{J} = \frac{1}{2}\dot{h}^2. \tag{40}$$

Differentiating $\mathcal{J}$ and recalling (36) yields

$$\dot{\mathcal{J}} = -kb(t)\frac{\dot{h}}{h}\left(\dot{h} + \alpha h\right). \tag{41}$$

It follows that $\mathcal{J}$ is negative as long as $|\dot{h}| > \alpha h$. Since there exists a time T such that $\dot{h} < 0\ \forall t > T$, it follows that $h > 0$ is upper bounded. Consequently, $\dot{h}$ is bounded.

Because of the variation of $b(t)$, boundedness of $\dot{h}$ is not sufficient to conclude that $\left|\int_0^t \frac{\ddot{h}(\tau)}{kb(\tau)}\, d\tau\right|$ is bounded. Therefore, it is necessary to study the evolution of $\ddot{h}$.

Proof that the sign of $\ddot{h}$ does not change more than once. In the following, we assume without loss of generality that $\dot{h}_0 < 0$; therefore, $\dot{h}(t) < 0$ for all time.

1) $\ddot{h}(0) \leq 0$: To show that there exists a time T such that $\ddot{h}(T) > 0$, assume the converse; that is, $\ddot{h} \leq 0$ for all time t. Since $\dot{h}$ is negative and decreasing, it follows that h is strictly monotonically decreasing and cannot have a positive limit. Consequently, from (36), there exists a time T such that $\dot{h}(T)/h(T) < -\alpha$. Hence, $\ddot{h}(T) > 0$, and the contradiction follows.
2) $\ddot{h}(0) > 0$: To show that $\ddot{h}(t) \geq 0$ for all time, assume the converse; that is, there exists T and $\delta > 0$ such that $\ddot{h}(T-\delta) = 0$ and $\dddot{h} < 0\ \forall t \in (T-\delta, T]$. This implies that $(\dot{h}/h)(T-\delta) = -\alpha$ and $\dot{h}/h > -\alpha\ \forall t \in (T-\delta, T]$. Using the fact that $\dot{h}/h = -\alpha$ at time $(T-\delta)$ and $|\dot{h}/h| < \alpha\ \forall t \in (T-\delta, T]$ while $\dot{h}$ is negative and decreasing and h is positive and decreasing, the contradiction follows.

Using the fact that there exists a time $T \in [0, T_{\max})$ from which $\dot{h} < 0$ is bounded and $\ddot{h} \geq 0,\ \forall t \in [T, T_{\max})$, it is straightforward to verify that $\left|\int_0^t \frac{\ddot{h}(\tau)}{kb(\tau)}\, d\tau\right|$ remains bounded on $[T, T_{\max})$. Therefore, since ζ is exponentially decreasing, one can ensure that h remains positive and exponentially decreasing on $[T, T_{\max})$.

Now, we prove that $T_{\max} = \infty$ and, thus, that ζ is well defined on $[0, \infty)$. Assume that $T_{\max} \neq \infty$, it means that there exists a positive number δ such that $h(t) > 0$ (by continuity) and such that $\left|\int_0^t \frac{\ddot{h}(\tau)}{kb(\tau)}\, d\tau\right|$ is unbounded on $[T_{\max}, T_{\max} + \delta)$. This contradicts the earlier discussion. It follows that h converges exponentially to 0. Moreover, using (40) and (41) with direct application of the input-to-state-stable argument, it follows that $\dot{h}$ is exponentially stable.

Proof of item 3 for $t \in [0, \infty)$:

Now, we prove that the controller (32) is bounded by proving that $\ddot{h} \to 0$. Analogously to the proof of Barbalat's Lemma, we proceed by contradiction. Assume that $\ddot{h}$ does not converge to 0. Since $\int_0^t (\dddot{h}/kb)(\tau)\, d\tau$ and $b(t)$ are bounded and there exists a time T such that $\dddot{h} \geq 0\ \forall t > T$, it follows that there exists $\epsilon > 0$ and two sequences $(T_n)_{n\geq 1} \in \mathbb{R}_+$ and $(\delta_n)_{n\geq 1} \in \mathbb{R}_+^*$ such that we have the following.

1) $T_n \to +\infty$ as $n \to +\infty$.
2) $\frac{\ddot{h}}{kb}(T_n - \delta_n) = \epsilon/2$ and $\frac{\ddot{h}}{kb}(T_n) = \epsilon$.
3) $\epsilon/2 \leq \frac{\ddot{h}}{kb}(t) \leq \epsilon,\ \forall t \in [T_n - \delta_n, T_n]$.

We need to show that $(\delta_n)_{n\geq 1}$ is lower bounded by a strictly positive number. Using the fact that $\ddot{h}/kb \leq \epsilon\ \forall t \in [T_n - \delta_n, T_n]$ and recalling (36), one has

$$\left(\frac{\dot{h}}{h} + \alpha\right) \geq -\epsilon.$$

Integrating this inequality within $[T_n - \delta_n, T_n]$, one obtains

$$\ln\left(\frac{h(t)}{h(T_n - \delta_n)}\right) \geq -\int_{T_n - \delta_n}^{t} (\alpha + \epsilon)\, d\tau.$$

Given that

$$-\int_{T_n - \delta_n}^{t} (\alpha + \epsilon)\, d\tau \geq -\int_{T_n - \delta_n}^{t} (\alpha_{\max} + \epsilon)\, d\tau$$

one has

$$\ln\left(\frac{h(t)}{h(T_n - \delta_n)}\right) \geq -(\alpha_{\max} + \epsilon)\,\delta_n.$$

Hence, $h(t) \geq h(T_n - \delta_n) \exp\left(-(\alpha_{\max} + \epsilon)\delta_n\right)\ \forall t \in [T_n - \delta_n, T_n]$, and therefore, using the fact that $\dot{h} < 0$ and increasing ($\ddot{h} \geq 0$)

$$\frac{\dot{h}}{h} \geq \frac{\dot{h}}{h(T_n - \delta_n)} \exp\left((\alpha_{\max} + \epsilon)\,\delta_n\right)$$

$$\frac{\dot{h}}{h} \geq \frac{\dot{h}(T_n - \delta_n)}{h(T_n - \delta_n)} \exp\left((\alpha_{\max} + \epsilon)\,\delta_n\right). \tag{42}$$

Using $(\dddot{h}/kb)(T_n - \delta_n) = \epsilon/2$ and $(\dddot{h}/kb)(T_n) = \epsilon$, one also has

$$\frac{\dot{h}}{h}(T_n) = -\epsilon - \alpha(T_n)$$

$$\frac{\dot{h}}{h}(T_n - \delta_n) = -\frac{\epsilon}{2} - \alpha(T_n - \delta_n).$$

Recalling inequality (42), it follows that

$$\exp\left((\alpha_{\max} + \epsilon)\,\delta_n\right) \geq \frac{\epsilon + \alpha(T_n)}{\epsilon/2 + \alpha(T_n - \delta_n)}.$$

Now, we need the uniform continuity of $\alpha(t)$. To show this, we first need to show that $1/b(t)$ is itself uniformly continuous [see (37)]. The result is straightforward to show using (31) and the fact that $(h, \dot{h})$ converge to 0 ($\dot{b}/b^2$ is bounded, and then, $1/b$ is uniformly continuous). Using assumptions of the theorem and the fact that $1/b$ is uniformly continuous, it follows that $\alpha(t)$ is uniformly continuous. Thus, there exists $\gamma > 0$ such that $|T_n - t| \leq \gamma \Rightarrow |\alpha(T_n) - \alpha(t)| \leq \epsilon/4$. Considering the case $\delta_n < \gamma$, one obtains $\alpha(T_n) \geq \alpha(T_n - \delta_n) - \epsilon/4$ and, therefore

$$\exp\left((\alpha_{\max} + \epsilon)\,\delta_n\right) \geq \frac{3\epsilon/4 + \alpha(T_n - \delta_n)}{\epsilon/2 + \alpha(T_n - \delta_n)}.$$

Using the fact that $\alpha(t)$ is bounded, it is straightforward to verify that

$$\frac{3\epsilon/4 + \alpha(t)}{\epsilon/2 + \alpha(t)} \geq \frac{3\epsilon/4 + \alpha_{\max}}{\epsilon/2 + \alpha_{\max}} \quad \forall t > 0.$$

This implies that

$$\exp\left((\alpha_{\max} + \epsilon)\,\delta_n\right) \geq \frac{3\epsilon/4 + \alpha_{\max}}{\epsilon/2 + \alpha_{\max}} > 1 \quad \forall n \geq 1.$$

Consequently, there exists $\delta > 0$ such that $\delta_n \geq \delta$ for all $n \geq 1$. The next step of the proof is a direct application of the proof of Barbalat's Lemma. By definitions (2) and (3) for all $t \in [T_n - \delta_n, T_n]$ and for all $n \geq 1$, we have

$$\begin{aligned}
\frac{\ddot{h}}{kb}(t) = \left|\frac{\ddot{h}}{kb}(t)\right| &= \left|\frac{\ddot{h}}{kb}(T_n) - \left(\frac{\ddot{h}}{kb}(T_n) - \frac{\ddot{h}}{kb}(t)\right)\right| \\
&\geq \left|\frac{\ddot{h}}{kb}(T_n)\right| - \left|\left(\frac{\ddot{h}}{kb}(T_n) - \frac{\ddot{h}}{kb}(t)\right)\right| \\
&\geq \epsilon - \frac{\epsilon}{2} \\
&\geq \frac{\epsilon}{2}.
\end{aligned}$$

As a consequence, $\int_0^t (\ddot{h}/kb)(\tau)\,d\tau$ converges to $+\infty$ which contradicts the hypothesis.

Using the fact that $\ddot{h}(t)$ converges to 0, it is straightforward to verify the following.

1) $\dot{h}/h \equiv -\alpha(t)$ when t tends to $+\infty$. This means that the descent speed depends on $\alpha(t)$.
2) $\ddot{h}$ is bounded, and therefore, the control law (32) is bounded. ■

Remark 5.2: Note that the stability of the control law (14) that is used for the lateral dynamics during the landing manoeuvre can also be proved in the case where $\Delta^{\parallel}$ and b are constant; the proof is similar to the second part of the proof of Theorem 4.1, using the fact that $\dot{h}$ is bounded and converges to 0. The authors do not have a formal proof of stability in the case where both $b(t)$ and $\Delta^{\parallel}(t)$ vary over time or in case where the lateral dynamics of the target plane is not zero. Nevertheless, if these variables vary sufficiently slowly ($\dot{b}(t) \approx 0$, $\dot{\Delta}^{\parallel}(t) \approx 0$, and $\dot{v}_t \approx 0$), then the robustness of Theorem 4.1 will ensure stability. To characterize the stability conditions is a difficult problem that remains open.

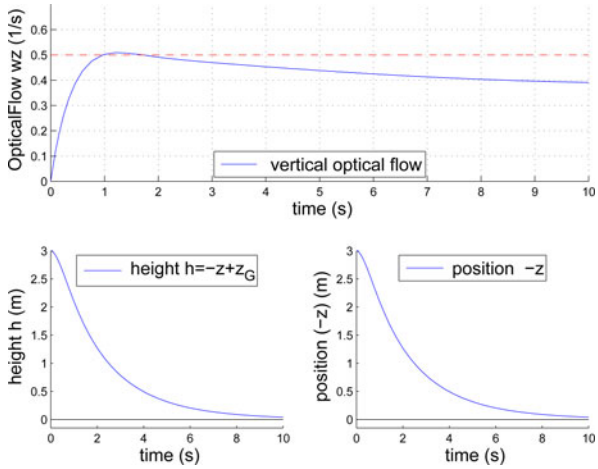

Fig. 5. Simulation of vertical landing on a static platform using controller (32).

VI. Simulations

In order to evaluate the efficiency of the proposed servo control technique, MATLAB simulations of the vertical landing of an idealized quadrotor (34) on static or moving platform are presented. The presented simulations consider only the vertical landing problem of the vehicle on a static and a moving platform.

The mass of the vehicle is chosen $m = 0.85$ kg. It corresponds to the physical mass of the quadrotor that is used for experiments. The control gain is set to $k = 10$, and the error Δ_z is chosen $\Delta_z = -0.3$. For the parameter b defined in (31), incorporating the ground effect, we have chosen $l_0 = 0.5$ m and $D_0 = 0.15$ m. The desired set point ω^* is set to 0.5 s^{-1}. Using the previous values of the different parameters that are involved in the vertical motion (36), it is straightforward to show that condition (33) is verified. Fig. 5 shows the closed-loop trajectory of the vertical motion of the vehicle. One can verify that the vertical optical flow w_z remains positive for all time, even if it does not reach ω^* and the height $h = -z + z_G$ converges exponentially to 0. We also notice that the height remains positive during the manoeuvre, which implies that the vehicle does not collide with the platform.

Fig. 6 shows the result with a moving platform. We keep the same parameters as earlier. The vertical motion of the platform is chosen as

$$z_G = a_G \sin(2\pi f_G t) \text{ with } a_G = 0.1\text{m and } f_G = 0.3\ \text{s}^{-1}.$$

It is straightforward to verify that condition (33) holds. Note that, during the simulation, z_G is assumed to be unknown. This means that no feed-forward compensations are performed. Fig. 6 shows the closed-loop trajectory of the vertical motion of the vehicle. Observe that the vertical optical flow remains positive for all time, even if it does not reach ω^*, and the height $h = -z + z_G$ converges exponentially to 0, despite the fact that the vertical motion of the platform is unknown. Fig. 7 shows the same result with an additional noise on the measured optical flow. One observes that the convergence is not affected, even close to the touchdown.

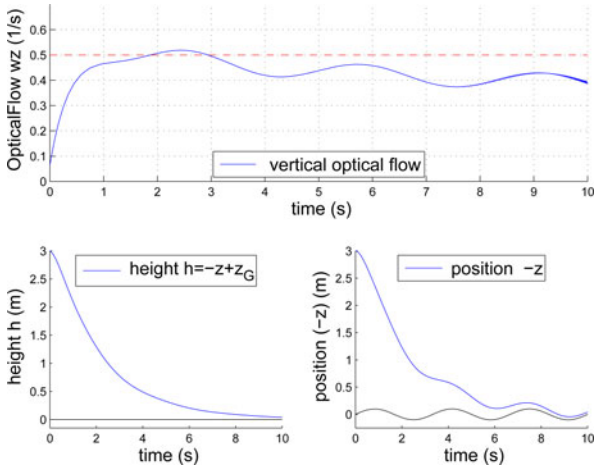

Fig. 6. Simulation of vertical landing on an oscillating platform using controller (32).

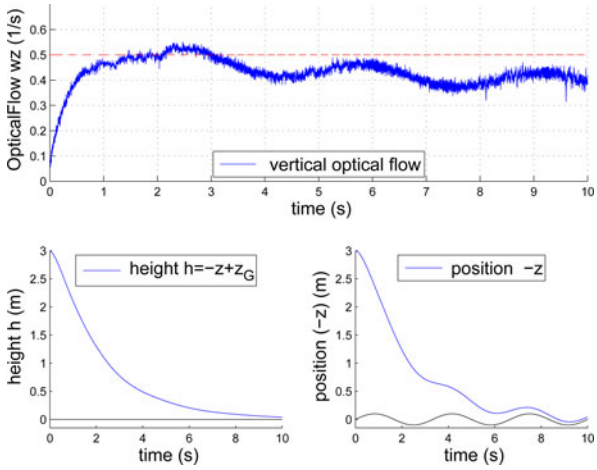

Fig. 7. Simulation of vertical landing on an oscillating platform with noisy optical flow.

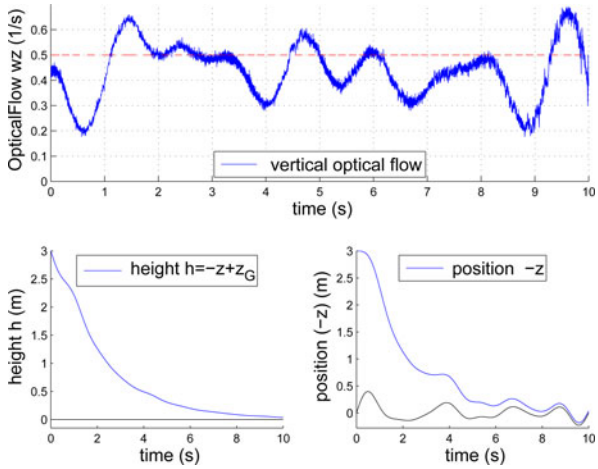

Fig. 8. Simulation of vertical landing on a stochastically moving platform using controller (32).

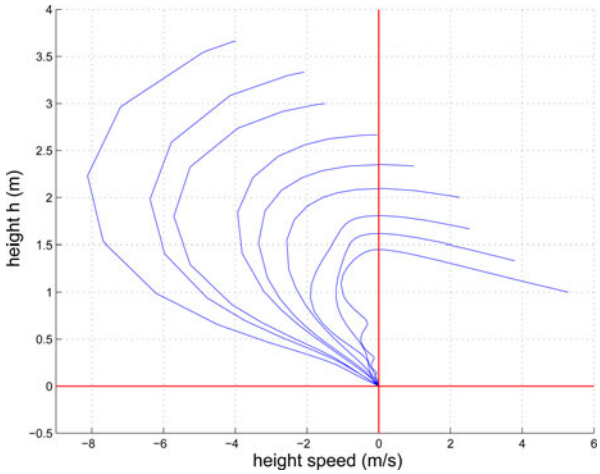

Fig. 9. Phase diagram of the dynamical system for nine independent simulations.

Fig. 8 shows the result with a stochastically moving platform. The vertical motion of the platform is now the sum of $n = 7$ sinusoidal signals [see (28)], where parameters $a_i \in [0, 0.1]$, $\omega_i \in [1, 6]$ and $\phi_i \in [0, 2\pi]$ are chosen stochastically. The bounds of the parameters are chosen to ensure that the condition (33) is verified. During the simulation, z_G is still assumed to be unknown. Once again, one observes the expected behavior: The height $h = -z + z_G$ converges exponentially to 0 despite the unknown motion of the platform.

In Fig. 9, a phase diagram for different trajectories is presented. For each trajectory, parameters are chosen stochastically and analogously to the previous simulation. $\Delta_z \in [-2, 2]$ is also chosen stochastically. As for the set point ω^* and initial conditions, they are chosen such that the figure is understandable: $h_0 \in [1, 4]$, $\dot{h}_0 \in [-4, 6]$, and $\omega^* \in [0.5, 4.5]$. Fig. 9 shows robustness of the approach since the expected behavior is observed for all trajectories. One can observe that the trajectories satisfy the result of Theorem 5.1, i.e., $h(t) > 0$ remains positive for all time and $(h, \dot{h})$ converge to zero. One also verifies that there exists a time $T \geq 0$ such that $\dot{h} < 0 \; \forall t \geq T$ (see the proof of the theorem).

VII. Experimental Results

In this section, we present two experiments that demonstrate the performance of the proposed control scheme on a physical vehicle. The UAV that is used for the experimentation is the quadrotor, constructed by the CEA (see Fig. 1), a VTOL vehicle that is ideally suited for stationary and quasi-stationary flight [28].

A. Prototype Description

The X4-flyer is equipped with a set of four electronic boards that are designed by the CEA. Each electronic board includes a microcontroller and has a particular function. The first board integrates motor controllers that regulate the rotation speed of the four propellers. The second board integrates an IMU that consists of three low-cost microelectromechanical systems accelerometers, which give the gravity components in the body

Fig. 10. Hovering flight above the landing pad.

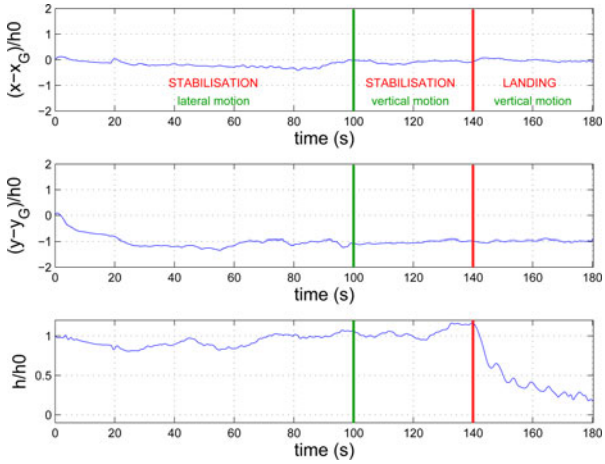

Fig. 11. Vertical landing on a moving platform.

frame, three angular rate sensors, and two magnetometers. On the third board, a digital signal processing (DSP), which is running at 150 MIPS, is embedded and performs the control algorithm of the orientation dynamics and filtering computations. The final board provides a serial wireless communication between the operator's joystick and the vehicle. An embedded camera with a view angle of 70° pointing directly down transmits video to a ground station (PC) via a wireless 2.4-GHz analog link. A lithium-polymer battery provides nearly 10 min of flight time. The loaded weight of the prototype is about 850 g. In parallel the video signal, the X4-flyer sends inertial data to the ground station at a frequency of 15 Hz. The data are processed by the ground station PC and incorporated into the control algorithm. Desired orientation and desired thrust are generated on the ground station PC and sent to the drone. A key challenge for the implementation lies in the relatively large time latency between the inertial data and visual features. For orientation dynamics, an embedded "high-gain" controller in the DSP, which is running at 166 Hz, independently ensures the exponential stability of the orientation toward the desired set point.

B. Experiments

The target plane that is used is a large board painted with random contrast textures (see Fig. 10). It is held and moved manually. A Pyramidal implementation of the Lucas–Kanade [29] algorithm is used to compute the optical flow. The efficiency of the algorithm is increased by defocusing the camera to low-pass filter images. The field of view of the aperture is of 30° around the direction of observation η. Optical flow is computed on 210 points on this aperture and a least-squares estimation of motion parameters is used to obtain robust measurements of the average optical flow w [30].

Given that the divergent flow magnitude is relatively small compared with the lateral flow in the forward and backward directions [31] and since only the divergent flow is used for landing manoeuvre, the control approach is split into two sequential phases. In the first phase, the vehicle is stabilized over the landing plane. Once the velocity has stablized to zero, the landing phase is initiated. During the experiments, the yaw velocity is also separately regulated to zero. This has no effect on the proposed control scheme. The landing pad has been moved both vertically and laterally to show performances of the control algorithms. For the vertical landing, the desired set point w^d is set to $(0, 0, 0.1)^T$. This ensures a relatively rapid descent (approximatively in 10 s).

Note that no measurements of the relative position $\tilde{\xi} = \xi - \xi_G$ of the UAV with respect to the platform are available. Nevertheless, an estimation of the UAV's relative position can be computed from the average optical flow using

$$\frac{\tilde{\xi} - \tilde{\xi}_0}{h_0} = \int_0^t w\gamma(\tau)\, d\tau = \int_0^t w \exp\left(-\int_0^\tau w_z\, d\delta\right) d\tau$$

where $\tilde{\xi}$ denotes the relative position of the UAV with respect to the platform: $\tilde{\xi} = \xi - \xi_G$. Note that

$$\gamma(\tau) = \exp\left(-\int_0^\tau w_z\, d\delta\right) = \exp\left(\int_0^\tau \frac{\dot{h}}{h}\, d\delta\right) = \frac{h(\tau)}{h_0}.$$

In Figs. 11 and 12, three components of the relative position $(\tilde{\xi} - \tilde{\xi}_0)/h_0$ are presented. Fig. 11 shows the result using controller (14) for the stabilization of the X4-flyer with respect to the platform (from 0 to 140 s) and controller (32) for the vertical landing manoeuvre (from 140 s). For the stabilization phase, the platform is moving laterally (from 0 to 100 s) and vertically (from 100 to 140 s). During the landing manoeuvre ($t \geq 140$ s), the platform is moving only vertically. Note that during the landing phase, controller (14) is still used for the x–y dynamics. This ensures that the vehicle remains stable over the landing pad. Fig. 11 shows the exponential descent of the height, while the lateral position remains stable. Note that the relative position $(y - y_G)/h_0$ converges around -1 because of an initial bias of the inertial measurements in y-direction that has been compensated by the integral term in the controller (14). Note also that, contrary to what was expected, the height h is slowly oscillating during the landing phase. This implies that condition (33) is not verified for all time t, and therefore, the positivity of

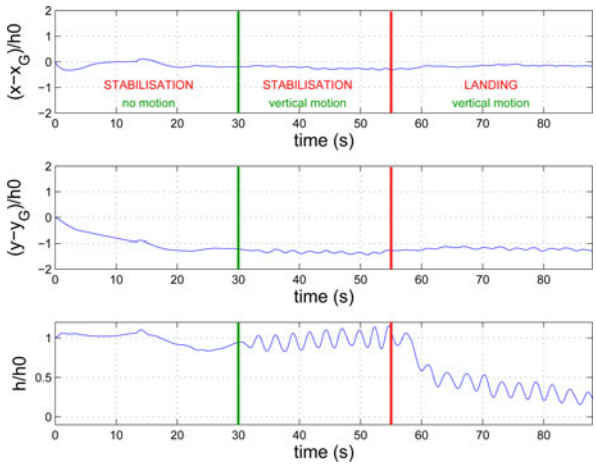

Fig. 12. Vertical landing with high oscillations.

$\alpha(t)$ (see Section V) is not always guaranteed. This problem is mainly because of the fact that experimental constraints (large time latency and outer loop's sampling time which is of 15 Hz) prevent us from choosing a higher gain k which strictly respect the condition. The vehicle lands at time 180 s. We notice that, because of the landing gear, the final position is not $h \equiv 0$.

Fig. 12 shows the result when the landing pad is moving with high oscillations. The controller for the stabilization of the X4-flyer with respect to the platform is used from 0 to 55 s, and the controller for landing is used from $t = 55$ s, while oscillations start from 30 s. During landing manoeuvre, the height h is highly oscillating, which means that the gain k is not high enough to compensate the oscillations. Nevertheless, the distance with the ground remains positive which ensures the noncollision with the moving target, and the UAV is even able to land with a satisfactory behavior.

These results can be watched on the video accompanying this paper or at the following url:
http://www.youtube.com/watch?v=hl18Fykax8M.

VIII. Concluding Remarks

This paper presented a nonlinear controller for vertical landing of a VTOL UAV using the measurement of average optical flow on a spherical camera along with the IMU data. The originality of our approach lies in the fact that neither linear velocity nor distance with the target is reconstructed. Inertial data are used only for *derotation* of the flow, and the proposed approach is an image-based visual control algorithm. Both stabilization and vertical landing with respect to a moving platform were considered, and a rigorous analysis of the stability of the closed-loop systems was provided. Simulations provide a clear picture of the predicted response of the proposed algorithm. The experimental results indicate some of the difficulties with obtaining high-gain feedback control and show that the proposed scheme is effective, even if the assumptions in the theorems do not necessarily hold.

There are several directions in which further work is of interest. The practical limitations of real-world systems limit magnitude of the feedback gain that can be applied and lead to limitations in the applicability of the approach in the presence of aggressive motion of the environment. Improving the time response of the optical sensors would already provide a major improvement in the closed-loop response and alleviate much of this difficulty. The consideration of a feed-forward compensation could alleviate the dependence on high-gain feedback when the environmental motion can be modeled. How to accomplish this within the image-based paradigm is a challenge. Finally, although the robustness of the proposed approach indicates that small variation of orientation and error in estimation of the normal direction will not destroy the obtained stability analysis, it is of interest to consider the situation where the platform orientation is time varying and where the normal of the platform is not assumed to be known.

Appendix

In this Appendix, we provide derivation of optical-flow integration that is described in (9) and used in Section III-B. Using the notations of Section III, consider the average of the optical flow in the direction η over a solid angle $\mathcal{W}^2$ of $\mathcal{S}^2$. Define (α_e, α_a) to be the spherical coordinates of η where α_e is the elevation angle and α_a is the azimuth angle. With these parameters, define R_t to be the orientation matrix from a frame of reference with η in the z-axis assuming no yaw rotation to the inertial frame $\mathcal{I}$[1]

$$R_t = \begin{pmatrix} \mathrm{c}(\alpha_e)c(\alpha_a) & -\mathrm{s}(\alpha_a) & \mathrm{s}(\alpha_e)\mathrm{c}(\alpha_a) \\ \mathrm{c}(\alpha_e)\mathrm{s}(\alpha_a) & \mathrm{c}(\alpha_a) & \mathrm{s}(\alpha_e)\mathrm{s}(\alpha_a) \\ -\mathrm{s}(\alpha_e) & 0 & \mathrm{c}(\alpha_e) \end{pmatrix}.$$

Define θ_0 as the angle associated with the apex angle $2\theta_0$ of the solid angle $\mathcal{W}^2$. Then

$$\phi = \iint_{\mathcal{W}^2} \dot{p}\, dp = -\pi \left(\sin\theta_0\right)^2 \Omega \times R^\top \eta - \frac{Q(V - V_t)}{d}$$

where $Q = R^\top (R_t \Lambda R_t^\top) R$ is a symmetric positive-definite matrix. The matrix Λ is a positive diagonal matrix depending on the solid angle $\mathcal{W}^2$. It can be written as

$$\begin{aligned} \Lambda &= \iint_{\mathcal{W}^2} \pi_q \langle p, R^\top \eta \rangle\, dq \\ &= \int_{\theta=0}^{\theta_0} \int_{\phi=0}^{2\pi} (I - qq^\top) \langle q, R_t^\top \eta \rangle \sin\theta\, d\theta\, d\phi \end{aligned}$$

where $q^\top = (\mathrm{s}(\theta)\mathrm{c}(\phi), \mathrm{s}(\theta)\mathrm{s}(\phi), \mathrm{c}(\theta))$. Eventually, straightforward but tedious calculations verify that

$$\Lambda = \frac{\pi \left(\sin\theta_0\right)^4}{4} \begin{pmatrix} \frac{1}{\lambda} & 0 & 0 \\ 0 & \frac{1}{\lambda} & 0 \\ 0 & 0 & 2 \end{pmatrix}$$

where $\lambda = \frac{(\sin\theta_0)^2}{4 - (\sin\theta_0)^2}$.

[1]for all $x \in \mathbb{R}, \mathrm{s}(x) = \sin(x), \mathrm{c}(x) = \cos(x), \mathrm{t}(x) = \tan(x)$.

REFERENCES

[1] K. P. Valavanis, *Advances in Unmanned Aerial Vehicles*. New York: Springer-Verlag, 2007.

[2] L. Marconi, A. Isidori, and A. Serrani, "Autonomous vertical landing on an oscillating platform: An internal-model based approach," *Automatica*, vol. 38, pp. 21–32, 2002.

[3] X. Yang, H. Pota, M. Garratt, and V. Ugrinovskii, "Prediction of vertical motions for landing operations of UAVs," presented at the 47th IEEE Conf. Decision Control, Cancun, Mexico, Dec. 2008.

[4] S.-R. Oh, K. Pathak, S. K. Agrawal, H. R. Pota, and M. Garratt, "Approaches for a tether-guided landing of an autonomous helicopter," *IEEE Trans. Robot.*, vol. 22, no. 3, pp. 536–544, Jun. 2006.

[5] S. Saripalli, J. F. Montgomery, and G. S. Sukhatme, "Visually-guided landing of an unmanned aerial vehicle," *IEEE Trans. Robot. Autom.*, vol. 19, no. 3, pp. 371–380, Jun. 2003.

[6] C. S. Sharp, O. Shakernia, and S. S. Sastry, "A vision system for landing an unmanned aerial vehicle," in *Proc. IEEE Int. Conf. Robot. Autom.*, 2001, pp. 1720–1727.

[7] M. V. Srinivasan, S. W. Zhang, J. S. Chahl, E. Barth, and S. Venkatesh, "How honeybees make grazing landings on flat surfaces," *Biol. Cybern.*, vol. 83, pp. 171–183, 2000.

[8] J. Koenderink and A. van Doorn, "Facts on optic flow," *Biol. Cybern.*, vol. 56, pp. 247–254, 1987.

[9] F. Ruffier and N. Franceschini, "Visually guided micro-aerial vehicle: Automatic take off, terrain following, landing and wind reaction," in *Proc. Int. Conf. Robot. Autom.*, New Orleans, LA, Apr. 2004, pp. 2339–2346.

[10] G. L. Barrows, J. S. Chahl, and M. V. Srinivasan, "Biomimetic visual sensing and flight control," presented at the Proc. 17th Int. Unmanned Air Veh. Syst. Conf., Bristol, U.K., Apr. 2002.

[11] A. Beyeler, J.-C. Zufferey, and D. Floreano, "Vision-based control of near-obstacle flight," *Auton. Robots*, vol. 27, no. 3, pp. 201–219, 2009.

[12] W. E. Green and P. Y. Oh, "Optic flow based collision avoidance," *IEEE Robot. Autom. Mag.*, vol. 15, no. 1, pp. 96–103, Mar. 2008.

[13] M. A. Garratt and J. S. Chahl, "Vision-based terrain following for an unmanned rotorcraft," *J. Field Robot.*, vol. 25, pp. 284–301, 2008.

[14] J. S. Humbert, R. M. Murray, and M. H. Dickinson, "Pitch-altitude control and terrain following based on bio-inspired visuomotor convergence," presented at the Proc. AIAA Conf. Guid., Navigat. Control, San Francisco, CA, 2005.

[15] F. Ruffier and N. Franceschini, "Optic flow regulation: The key to aircraft automatic guidance," *Robot. Auton. Syst.*, vol. 50, pp. 177–194, 2005.

[16] R. Mahony, P. Corke, and T. Hamel, "Dynamic image-based visual servo control using centroid and optic flow features," *J. Dyn. Syst. Meas. Control*, vol. 130, no. 1, 011005 (12 pp.), 2008.

[17] F. Kendoul, I. Fantoni, and K. Nonami, "Optic flow-based vision system for autonomous 3D localization and control of small aerial vehicles," *Robot. Auton. Syst.*, vol. 57, no. 6–7, pp. 591–602, 2009.

[18] S. Bertrand, T. Hamel, and H. Piet-Lahanier, "Stability analysis of an UAV controller using singular perturbation theory," presented at the 17th IFAC World Congr., Seoul, Korea, Jul. 2008.

[19] B. Hérissé, T. Hamel, R. Mahony, and F-X. Russotto, "The landing problem of a VTOL unmanned aerial vehicle on a moving platform using optical flow," in *Proc. IEEE/RSJ Int. Conf. Intell. Robots Syst.*, Taipei, Taiwan, Oct. 2010, pp. 1600–1605.

[20] R. Mahony and T. Hamel, "Robust trajectory tracking for a scale model autonomous helicopter," *Int. J. Non-linear Robust Control*, vol. 14, pp. 1035–1059, 2004.

[21] H. K. Khalil, *Nonlinear Systems*, 2nd ed. Englewood Cliffs, NJ: Prentice-Hall, 1996.

[22] T. Hamel and R. Mahony, "Visual servoing of an under-actuated dynamic rigid-body system: An image based approach," *IEEE Trans. Robot. Autom.*, vol. 18, no. 2, pp. 187–198, Apr. 2002.

[23] R. F. Vassallo, J. Santos-Victor, and H. J. Schneebeli, "A general approach for egomotion estimation with omnidirectional images," in *Proc. Omnidirectional Vis.*, Copenhagen, Denmark, Jun. 2002, pp. 97–103.

[24] J. L. Barron, D. J. Fleet, and S. S. Beauchemin, "Performance of optical flow techniques," *Int. J. Comput. Vis.*, vol. 12, no. 1, pp. 43–77, 1994.

[25] N. Metni, J. M. Pflimlin, T. Hamel, and P. Souares, "Attitude and gyro bias estimation for a flying UAV," in *Proc. IEEE Int. Conf. Intell. Robots Syst.*, Edmonton, AB, Canada, 2005, pp. 1114–1120.

[26] C. McCarthy, N. Barnes, and R. Mahony, "A robust docking strategy for a mobile robot using flow field divergence," *IEEE Trans. Robot.*, vol. 24, no. 4, pp. 832–842, Aug. 2008.

[27] N. Guenard, *Optimisation et implémentation de lois de commande embarquées pour la téléopération intuitive de micro drones aériens "X4-flyer*," Ph.D. dissertation, Univ. Nice Sophia Antipolis, Sophia Antipolis, France, 2007.

[28] N. Guenard, T. Hamel, and R. Mahony, "A practical visual servo control for an unmanned aerial vehicle," *IEEE Trans. Robot.*, vol. 24, no. 2, pp. 331–340, Apr. 2008.

[29] B. Lucas and T. Kanade, "An iterative image registration technique with an application to stereo vision," in *Proc. 7th Int. Joint Conf. Artif. Intell.*, Vancouver, BC, Canada, 1981, pp. 674–679.

[30] S. Umeyama, "Least-squares estimation of transformation parameters between two point patterns," *IEEE Trans. Pattern Anal. Mach. Intell.*, vol. 13, no. 4, pp. 376–380, Apr. 1991.

[31] J. S. Chahl and M. V. Srinivasan, S. W. Zhang, "Landing strategies in honeybees and applications to uninhabited airborne vehicles," *Int. J. Robot. Res.*, vol. 23, no. 2, pp. 101–110, 2004.

Bruno Hérissé received the Engineer degree from the École Supérieure d'Électricité (SUPELEC), a French "Grande École" of Engineering in energy and information science, Paris, France, in 2007, and the Research Master degree in signal, telecommunications, and image processing from SUPELEC in joint authorization with the University of Rennes 1, Rennes, France, in 2007. After three years of research with the Interactive Robotics Laboratory at CEA List, he received the Ph.D. degree in robotics from the University of Nice Sophia Antipolis, Sophia Antipolis, France, in 2010.

He has been a Research Engineer with ONERA, the French Aerospace Lab, Palaiseau, France, since 2011. His current research interests include localization and navigation of unmanned aerial vehicles.

Tarek Hamel received the Engineer degree in automatic control from the Institut d'Electronique et d'Automatique d'Annaba, Annaba, Algeria, in 1991 and the Ph.D. degree in robotics from the University of Technologie of Compiègne, Compiègne, France in 1995.

After two years as a Research Assistant with the University of Technology of Compiègne, he joined the Centre d'Etudes de Mècanique d'Iles de France in 1997 as an Associate Professor. In 2001/2002, he spent one year as a CNRS Researcher with the Heudiasyc Laboratory. Since 2003, he has been a Full Professor with the I3S UNSA-CNRS Laboratory, University of Nice Sophia Antipolis, Sophia Antipolis, France. His research interests include control theory and robotics with particular focus on nonlinear control, vision-based control, and estimation and filtering on Lie groups. He is involved in applications of these techniques to the control of unmanned aerial vehicles and mobile robots.

Robert Mahony received the Bachelor of Science degree from the Australian National University (ANU), Canberra, Australia, in 1989, where he studied applied mathematics and geology. After working for a year as a geophysicist processing marine seismic data, he returned to study at ANU and received the Ph.D. degree in systems engineering in 1994.

Between 1994 and 1997, he was a Research Fellow with the Cooperative Research Centre for Robust and Adaptive Systems based in the Research School of Information Sciences and Engineering, ANU. From 1997 to 1999, he was a Postdoctoral Fellow with the CNRS Laboratory for Heuristics Diagnostics and Complex Systems, Compiegne University of Technology, Compiegne, France. Between 1999 and 2001, he held a Logan Fellowship with the Department of Engineering and Computer Science, Monash University, Melbourne, Australia. In July 2001, he took a faculty position with the Research School of Engineering, ANU. His research interests include nonlinear control theory with applications in mechanical systems and motion systems, mathematical systems theory and geometric optimization techniques with applications in linear algebra, and digital signal processing.

François-Xavier Russotto received the Graduate Engineering degree from the École Supérieure d'Électricité (SUPELEC), a French "Grande École" of Engineering in Energy and Information Science, Paris, France, in 1997.

He worked for four years as a Design Engineer at Thales Optronics SA (TOSA), on the design of servomechanisms for aircraft embedded systems. In 2001, he joined Peugeot Citroen Automobiles SA (PSA) as a Project Manager, working on design of innovative prototypes of by-wire Man-Machine Interface for tourism vehicles. Since 2002, he has been at CEA LIST Labs, first as a project manager in Robotics R&D, where he started working on the design of embedded control software for computer aided teleoperation systems. Since 2006, he has held the position of technical project manager responsible for R&D activity focused on virtual reality-based supervisory control software for teleoperation systems.